Comparison of algorithms for incoming atmospheric long-wave radiation

G. N. Flerchinger,[1] Wei Xaio,[2] Danny Marks,[1] T. J. Sauer,[3] and Qiang Yu[2]

Received 27 August 2008; revised 26 January 2009; accepted 11 February 2009; published 31 March 2009.

[1] While numerous algorithms exist for predicting incident atmospheric long-wave radiation under clear (L_{clr}) and cloudy skies, few comparisons have been published to assess the accuracy of the different algorithms. Virtually no comparisons have been made for both clear and cloudy skies across multiple sites. This study evaluates the accuracy of 13 algorithms for predicting incident long-wave radiation under clear skies, ten cloud correction algorithms, and four algorithms for all-sky conditions using data from 21 sites across North America and China. Data from five research sites were combined with publicly available data from nine sites in the AmeriFlux network for initial evaluation and optimization of cloud cover estimates; seven additional AmeriFlux sites were used as an independent test of the algorithms. Clear-sky algorithms that excelled in predicting L_{clr} were the Dilley, Prata, and Ångström algorithms. Root mean square deviation (RMSD) between predicted and measured 30-minute or hourly L_{clr} averaged approximately 23 W m^{-2} for these three algorithms across all sites, while RMSD of daily estimates was as low as 14 W m^{-2}. Cloud-correction algorithms of Kimball, Unsworth, and Crawford described the data best when combined with the Dilley clear-sky algorithm. Average RMSD across all sites for these three cloud corrections was approximately 24 to 25 W m^{-2} for 30-minute or hourly estimates and approximately 15 to 16 W m^{-2} for daily estimates. The Kimball and Unsworth cloud corrections require an estimate of cloud cover, while the Crawford algorithm corrects for cloud cover directly from measured solar radiation. Optimum limits in the clearness index, defined as the ratio of observed solar radiation to theoretical terrestrial solar radiation, for complete cloud cover and clear skies were suggested for the Kimball and Unsworth algorithms. Application of the optimized algorithms to seven independent sites yielded similar results. On the basis of the results, the recommended algorithms can be applied with reasonable accuracy for a wide range of climates, elevations, and latitudes.

Citation: Flerchinger, G. N., W. Xaio, D. Marks, T. J. Sauer, and Q. Yu (2009), Comparison of algorithms for incoming atmospheric long-wave radiation, *Water Resour. Res.*, *45*, W03423, doi:10.1029/2008WR007394.

1. Introduction

[2] Downwelling long-wave radiation is vitally important for numerous applications requiring surface radiation and energy balance, including predicting evapotranspiration, snowmelt, surface temperature, and frost occurrence. Meteorological stations rarely include long-wave radiation sensors, so measurements of incoming long-wave radiation are generally not available for a given location and period of interest. While surface radiative fluxes can be calculated with reasonable accuracy using complex radiative transfer models [*Edwards and Slingo*, 1996; *Pope et al.*, 2000], these require detailed measurements of the air column above a site, including cloud properties and vertical profiles of temperature, water vapor, trace gases, and aerosols. Because these measurements are rarely available, downwelling long-wave radiation is commonly estimated from algorithms that use more readily available meteorological observations, such as air temperature, humidity, and solar radiation. Although these simpler algorithms may have larger errors relative to the more complex methods, these methods are needed and are useful for a variety of disciplinary applications, despite the small errors.

[3] Several parameterizations have been developed that produce estimates for downwelling long-wave radiation (L_d) using synoptic observations [e.g., *Idso and Jackson*, 1969; *Maykut and Church*, 1973; *Jacobs*, 1978; *Idso*, 1981; *Aubinet*, 1994; *Dilley and O'Brien*, 1998; *Duarte et al.*, 2006; *Lhomme et al.*, 2007]. However, the few studies that offer a comparison of the different algorithms against measured L_d do not include more than two or three sites [*Alados-Alboledas et al.*, 1995; *Orsini et al.*, 2000; *Niemelä et al.*, 2001; *Iziomon et al.*, 2003; *Pérez-García*, 2004]. *Hatfield et al.* [1983] and *Finch and Best* [2004] did evaluate algorithms for multiple locations. *Hatfield et al.* [1983] compared several algorithms for clear skies at 15

[1]USDA Agricultural Research Service, Northwest Watershed Research Center, Boise, Idaho, USA.
[2]Institute of Geographical Sciences and Natural Resources Research, Chinese Academy of Sciences, Beijing, China.
[3]National Soil Tilth Laboratory, USDA Agricultural Research Service, Ames, Iowa, USA.

0043-1397/09/2008WR007394$09.00

Table 1. Algorithms for Estimating Clear-Sky Emissivity Following the Form of the Stefan-Boltzmann Equation or for Estimating Downwelling Long-wave Radiation Directly[a]

Source	Clear-Sky Algorithm
Ångström [1918][b]	$\varepsilon_{clr} = \left(0.83 - 0.18 \times 10^{-0.067 e_o}\right)$
Brunt [1932][b]	$\varepsilon_{clr} = (0.52 + 0.205\sqrt{e_o})$
Brutsaert [1975]	$\varepsilon_{clr} = 1.723\left(\frac{e_o}{T_o}\right)^{1/7}$
Garratt [1992]	$\varepsilon_{clr} = 0.79 - 0.17 \exp(-0.96 e_o)$
Idso and Jackson [1969]; referred to as Idso-1	$\varepsilon_{clr} = 1 - 0.261 \exp(-0.00077(T_o - 273.16)^2)$
Idso [1981]; referred to as Idso-2	$\varepsilon_{clr} = 0.7 + 5.95 \times 10^{-4} e_o \exp\left(\frac{1500}{T_o}\right)$
Iziomon et al. [2003][d]	$\varepsilon_{clr} = 1 - X \exp\left(\frac{-Y e_o}{T_o}\right)$
Keding [1989]	$\varepsilon_{clr} = 0.92 - 0.7 \times 10^{-1.2 e_o}$
Niemelä et al. [2001]	$\varepsilon_{clr} = \begin{cases} 0.72 + 0.09(e_o - 0.2) & for \quad e_o \geq 0.2 \\ 0.72 - 0.76(e_o - 0.2) & for \quad e_o < 0.2 \end{cases}$
Prata [1996][c]	$\varepsilon_{clr} = 1 - (1 + w) \exp(-(1.2 + 3w)^{1/2})$
Satterlund [1979]	$\varepsilon_{clr} = 1.08[1 - \exp(-(10 e_o)^{T_o}/2016)]$
Swinbank [1963]	$L_{clr} = 5.31 \times 10^{-13} T_o^6$
Dilley and O'Brien [1998][c]	$L_{clr} = 59.38 + 113.7\left(\frac{T_o}{273.16}\right)^6 + 96.96\sqrt{w/25}$

[a]Coefficients are based on vapor pressure (e_o) in kilopascals, temperature (T_o) in kelvins, and precipitable water (w) in centimeters.
[b]As cited by *Niemelä et al.* [2001].
[c]$w = 4650 e_o/T_o$ [*Prata*, 1996].
[d]Values for X and Y in the algorithm of *Iziomon et al.* [2003] were interpolated between a lowland site at 212-m elevation ($X = 0.35$ and $Y = 100$ K kPa^{-1}) and a mountain site at 1489-m elevation ($X = 0.43$ and $Y = 115$ K kPa^{-1}).

locations across the United States with measured L_d; *Finch and Best* [2004] compared five algorithms for L_d against values predicted by the radiation transfer scheme within a climate model to determine their suitability for global applications. However, *Finch and Best* [2004] did not use measured L_d and neither of these comparisons considered any of the available cloud cover corrections.

[4] Broad-scale comparisons of L_d algorithms are not available, in part, because of the relative scarcity of data sets that include measurements of L_d. However, the availability of AmeriFlux data make L_d measurements available for numerous sites, representing a broad range of climates. The purpose of this paper was to: compare a variety of algorithms for estimating clear and cloudy sky incoming long-wave radiation across numerous sites representing a variety of climates; determine which algorithms work best; and evaluate the error for different algorithms.

2. Parameterization Schemes

[5] Downwelling long-wave radiation is the thermal radiation emitted by the atmosphere downward to the ground surface. It is often computed from a general equation following the form of Stefan-Boltzmann equation.

$$L_d = \varepsilon_{eff} \sigma T_{eff}^4 \tag{1}$$

where ε_{eff} and T_{eff} (K) are the effective emissivity and temperature of the atmosphere above the site, and σ is the Stefan-Boltzmann constant. The temperature and emissivity are integrated quantities over an atmospheric column above the site and are typically estimated from ground-based meteorological observations only.

2.1. Clear-Sky Parameterizations

[6] Typically, long-wave parameterizations use near-surface air temperature and humidity measurements to calculate clear-sky fluxes based on the Stefan-Boltzmann equation.

$$L_{clr} = \varepsilon_{clr} \sigma T_o^4 \tag{2}$$

where L_{clr} is the incoming long-wave radiation for clear skies, ε_{clr} is the clear-sky emissivity, and T_o is near-surface air temperature (K). Several algorithms have been developed to estimate downward surface long-wave radiation flux using synoptic observations only. We assessed 13 algorithms given in Table 1 for estimating clear-sky downwelling long-wave flux (L_{clr}). In this article, the unit of the radiative flux is W m^{-2}, the unit of vapor pressure (e_o) is kPa, and the unit of T_o is K.

2.2. Elevation Corrections

[7] Elevation can affect L_d because the air column above the site decreases with elevation. *Deacon* [1970] developed an elevation correction based on the clear-sky equation of *Swinbank* [1963]. It is expressed as

$$L_{clr-elev} = L_{clr} - 0.035\left(\frac{z}{1000}\right)\sigma T_o^4 \tag{3}$$

where z is elevation of the site in meters a.m.s.l., however this expression was developed using data to no more than 1700 m.

[8] *Marks and Dozier* [1979] developed an elevation correction based on the clear-sky equation of *Brutsaert* [1975].

$$\varepsilon_{clr} = \left[1.723\left(\frac{e'}{T'}\right)^{1/7}\right] \times \left(\frac{P_o}{P_{sl}}\right). \tag{4}$$

Here, e' and T' are vapor pressure and temperature adjusted to their sea level equivalents assuming a standard lapse rate and constant humidity, P_o is air pressure at the site and P_{sl} is sea level air pressure (101.3 kPa). This expression was

Table 2. Algorithms for Correcting Clear-Sky Emissivity or Clear-Sky Long-Wave Radiation for Cloudy Skies

Source	Cloud-Correction Algorithm
	Algorithms Based on Cloud Cover, c
Brutsaert [1982]	$\varepsilon_a = (1 + 0.22c)\varepsilon_{clr}$
Iziomon et al. [2003][a]	$\varepsilon_a = (1 + Zc^2)\varepsilon_{clr}$
Jacobs [1978]	$\varepsilon_a = (1 + 0.26c)\varepsilon_{clr}$
Keding [1989]	$\varepsilon_a = (1 + 0.153c^{2.183})\varepsilon_{clr}$
Maykut and Church [1973]	$\varepsilon_a = (1 + 0.22c^{2.75})\varepsilon_{clr}$
Sugita and Brutsaert [1993]	$\varepsilon_a = (1 + 0.0496c^{2.45})\varepsilon_{clr}$
Unsworth and Monteith [1975]	$\varepsilon_a = (1 - 0.84c)\varepsilon_{clr} + 0.84c$
Kimball et al. [1982]	$L_d = L_{clr} + \tau_8 c f_8 \sigma T_c^4$ $\tau_8 = 1 - \varepsilon_{8z}(1.4 - 0.4\varepsilon_{8z})$ $\varepsilon_{8z} = 0.24 + 2.98 \times 10^{-6} e_o^2 \exp\left(\frac{3000}{T_o}\right)$ $f_8 = -0.6732 + 0.6240 \times 10^{-2} T_c - 0.9140 \times 10^{-5} T_c^2$
	Algorithms Based on Solar Index, s
Crawford and Duchon [1999]	$\varepsilon_a = (1 - s) + s\varepsilon_{clr}$
Lhomme et al. [2007]	$\varepsilon_a = (1.37 - 0.34s)\varepsilon_{clr}$

[a]Values for Z in the algorithm of *Iziomon et al.* [2003] were extrapolated from values $Z = 0.35$ for a site at 212-m elevation and 0.50 for a site at 1489-m elevation.

developed using periodic clear-sky data from 26 sites ranging in elevation from 2929 to 3750 m across the southern Sierra Nevada Mountains of California.

[9] *Iziomon et al.* [2003] reported different parameter values for their algorithm based on sites at different elevations. Herein, parameters for the Iziomon algorithm were extrapolated from those reported for a lowland site and a mountain site (Table 1).

2.3. Estimates of Cloud Cover

[10] Clear-sky long-wave radiation computed from algorithms in Table 1 must be adjusted for cloud cover. Most approaches adjust ε_{clr} for the fraction of cloud cover, c, to compute an effective atmospheric emissivity, ε_a. Cloudiness can be estimated from a clearness index (k), defined herein as the ratio of solar radiation flux density (S_t) to total hemispherical solar radiation flux density incident on a horizontal surface at the outer edge of the earth's atmosphere (S_o). *Campbell* [1985] suggests that c can be linearly interpolated between $c = 1.0$ at a clearness index of 0.4 for complete cloud cover (k_{cld}) to $c = 0.0$ at a clearness index of 0.7 (k_{clr}). Others have used values of 0.35 and 0.6 for k_{cld} and k_{clr}, respectively [*Flerchinger*, 2000; *Xiao et al.*, 2006]; the optimum values are unknown and may perhaps depend on the location.

[11] Alternatively, *Kasten and Czeplak* [1980] proposed a relation between cloud cover and solar radiation of the form

$$S_t = S_{clr}\left(1 - b_1 c^{b_2}\right) \tag{5}$$

where S_{clr} is incoming short-wave radiation for clear-sky conditions. They obtained values of 0.75 and 3.4 for b_1 and b_2 using data recorded in Hamburg, Germany over a 10-year period. The above equation can be rearranged to compute cloud cover by

$$c = \left(\frac{1 - k/k_{clr}}{b_1}\right)^{1/b_2} \tag{6}$$

where k_{clr} is the clearness index for clear-sky conditions.

[12] The period over which solar radiation is accumulated for calculating k poses a problem for estimates at nighttime and low sun angles. Instantaneous readings are not usable at night, and small errors in solar radiation measurements at low sun angles can significantly bias estimates of k. Additionally, daytime 30-minute or hourly solar readings may not necessarily be representative as clouds covering the solar disk may not be indicative of the entire hemispherical cloud cover. While some have limited their analyses to daytime observations [*Crawford and Duchon*, 1999], others have used average clearness estimates over a 2.5-hour window during the previous midafternoon for nighttime values [*Lhomme et al.*, 2007], or solar radiation averaged over the entire day of observation [*Flerchinger*, 2000].

2.4. Cloudy-Sky Corrections

[13] Ten cloud-correction algorithms presented in Table 2 were assessed. Most algorithms adjust ε_{clr} for cloud cover to compute ε_a. Because the clear-sky equations of *Swinbank* [1963] and *Dilley and O'Brien* [1998] are not based on a clear-sky emissivity (Table 1), it was necessary to back-calculate ε_{clr} from their estimates of L_{clr} before applying the equations in Table 2. To avoid the complication of estimating cloud cover, *Crawford and Duchon* [1999] and *Lhomme et al.* [2007] based their cloud corrections on the ratio of measured solar radiation (S_t) to the clear-sky irradiance (S_{clr}): $s = S_t/S_{clr}$, referred to herein as a solar index. The approach used by *Crawford and Duchon* [1999] for estimating S_{clr} for a given site and time of year is given in Appendix A.

[14] *Kimball et al.* [1982] presented a cloud cover correction for multiple cloud layers within the atmosphere. Herein, Kimball's approach was simplified to a single cloud layer with a fractional cover c, emissivity of 1.0, and temperature T_c. For this exercise, T_c was assumed to average 11 K cooler than air temperature at the surface with a seasonal variation of ±2 K, higher in summer than in winter [*Unsworth and Monteith*, 1975]. While *Kimball et al.* [1982] indicates that thin cloud types, such as cirrus, have emissivities averaging 0.5, their solar transmissivity will

Table 3. Algorithms for Directly Computing Long-Wave Radiation for All-Sky Conditions Based on Vapor Pressure (e_o in Kilopascals), Temperature (T_o in Kelvins), and Clearness Index (k)

Name	All-Sky algorithms
Aubinet-1	$L_d = \sigma(-29 + 1.09T_o - 19.9k)^4$
Aubinet-2	$L_d = \sigma(94 + 12.6\ \ln(1000e_o) - 0.13k + 0.341T_o)^4$
Aubinet-3	$L_d = \sigma(154 + 17.7\ \ln(1000e_o) - 9.93k)^4$
Aubinet-4	$L_d = (0.682 + 0.0352\ \ln(1000e_0) + 0.133\ \ln[1 - k])\sigma T_0^4$

also be higher, resulting in an underestimate of cloud cover based on k or s. These errors will tend to compensate for each other, resulting in relatively small errors in assuming 1.0 for cloud emissivity.

[15] Four additional schemes for directly estimating downward long-wave radiation of variably cloudy skies introduced by *Aubinet* [1994] were also evaluated. These are presented in Table 3. Each of the algorithms of *Aubinet* [1994] uses a different combination of temperature, vapor pressure and clearness index depending on data availability.

3. Methods

[16] Data collected from five separate sites were combined with nine AmeriFlux sites to develop a data set for initial evaluation and optimization of the long-wave radiation algorithms. Seven additional Ameriflux sites were used for an independent test of the algorithms. In most cases, two years of data were used for analysis. Basic climatic characteristics of each site are summarized in Table 4.

[17] The Idaho site is Reynolds Mountain located on the Reynolds Creek Experimental Watershed operated by the USDA Agricultural Research Service. The site is semiarid rangeland characterized by a Mediterranean climate. Data were used from three sites in China. The Yucheng Comprehensive Experiment Station of the Chinese Academy of Sciences lies on the North China Plain and is subject to a monsoonal climate. Measurements were collected at Yucheng above an irrigated wheat/maize field. Ganzi and Nagqu are two high-elevation semiarid grassland sites on the Tibetan Plateau. Data from Iowa were collected on the Brooks field near Ames, IA, a humid midcontinental site. Like most of the AmeriFlux sites, temperature and humidity at the Idaho, Iowa and Yucheng sites were collected using an HMP45 humidity probe (Vaisala, Helsinki, Finland), and incoming solar and long-wave radiation at the Iowa and China sites were measured using an unventilated, unheated, four-component net radiometer (CNR-1, Kipp and Zonen, Delft, Netherlands), calibrated every couple years. A newly calibrated CG3 pyrgeometer, which is the same sensor used for long-wave radiation in the CNR-1, was installed in 2003 at the Idaho site. Data from Idaho and Iowa are 30-minute averages, and data from Yucheng, China are hourly averages. *Michel et al.* [2008] reported accuracies of 16 W m^{-2} for hourly averages and 12 W m^{-2} for daily averages for the downward long-wave component of unheated, unventilated CNR-1 radiometers. Radiation data from Ganzi and Nagqu were collected using a pyrheliometer (MS-52, EKO, Japan) and an Eppley Precision Infrared Radiometer calibrated prior to the experiment and comparatively checked afterward. Temperature and humidity were measured using an aspirated psychrometer.

[18] Data from the AmeriFlux sites were downloaded from the Web interface located at http://public.ornl.gov/ameriflux/. Sites were screened using the graphing interface for those sites that collect incoming long-wave radiation and have two years of relatively high-quality temperature, humidity, solar radiation and long-wave radiation data, while trying to cover a broad range of climates and geographic regions. The sites selected for initial evaluation

Table 4. Characteristics of Sites Used for Testing Algorithms[a]

Location	Latitude/Longitude	Elevation (m)	Average Air Temperature (°C)	Average Vapor Deficit (kPa)	Average Clearness Index	Average L_d (W m^{-2})	Period
Sites Used for Initial Evaluation and Optimization							
Arizona	31° 49′N 110° 52′W	1120	19.7	1.83	0.66	325	Jan 2004 to Dec 2005
British Columbia	49° 52′N 125° 20′W	300	8.0	0.26	0.40	312	Jan 2000 to Dec 2001
Colorado	40° 02′N 105° 33′W	3050	3.0	0.50	0.60	259	Jan 2000 to Dec 2001
Ganzi, China	31° 37′N 100° 00′E	3394	6.7	0.58	0.63	281	Aug 1982 to Jul 1983
Idaho	43° 04′N 116° 45′W	2097	6.1	0.62	0.59	274	Jan 2005 to Dec 2006
Indiana	39° 19′N 86° 25′W	285	12.1	0.44	0.49	329	Jan 2003 to Dec 2004
Iowa	41° 58′N 96° 42′W	313	11.7	0.55	0.54	323	Jun 2005 to Dec 2006
Mississippi	34° 15′N 89° 58′W	70	16.2	0.49	0.52	337	Jan 2004 to Dec 2005
Nagqu, China	31° 29′N 92° 03′E	4505	3.1	0.44	0.58	258	Aug 1982 to Jul 1983
North Carolina	35° 59′N 79° 6′W	163	15.0	0.57	0.52	327	Jan 2004 to Dec 2005
South Dakota	44° 9′N 130° 39′W	1750	6.1	0.59	0.58	276	Jan 2004 to Dec 2005
Washington	45° 49′N 121° 57′W	371	10.0	0.41	0.47	324	Jan 2003 to Dec 2004
Wisconsin	45° 48′N 90° 05′W	520	6.7	0.15	0.49	306	Jan 2004 to Dec 2005
Yucheng, China	36° 50′N 116° 34′E	28	16.0	0.63	0.43	338	Jun 2003 to Nov 2004
Sites Used for Independent Testing							
Alaska	68° 29′N 155° 45′W	579	1.1	0.21	0.53	275	Jan 2005 to Dec 2006
Arizona	35° 5′N 111° 46′W	2215	8.7	0.77	0.67	264	Jan 2006 to Dec 2007
Illinois	42° 0′N 88° 18′W	300	10.7	0.37	0.52	307	Jan 2004 to Dec 2004
Missouri	38° 45′N 92° 12′W	216	14.2	0.76	0.54	322	Jan 2006 to Dec 2007
Montana	48° 18′N 105° 6′W	634	5.8	0.56	0.56	270	Jan 2005 to Dec 2006
South Dakota	44° 21′N 96° 50′W	510	7.4	0.39	0.57	294	Dec 2004 to Nov 2006
Tennessee	35° 58′N 84° 17′W	370	13.6	0.54	0.49	331	Jan 2003 to Jun 2004

[a]Averages represent the data used for analysis and may not reflect annual averages due to data gaps and incomplete years.

included: Santa Rita, Arizona; Campbell River, British Columbia; Niwot Ridge, Colorado; Morgan Monroe State Forest, Indiana; Goodwin Creek, Mississippi; Duke Forest (pine site), North Carolina; Black Hills, South Dakota; Wind River Crane Site, Washington; and Willow Creek, Wisconsin. Seven additional sites used as an independent test of the optimized clearness indices included: Ivotuk, Alaska; Flagstaff, Arizona; Bondville, Illinois; Missouri Ozark; Fort Peck, Montana; Bismark, South Dakota; and Walker Branch, Tennessee. Measurements at all sites were at least two meters above the vegetation. Data from the sites were 30-minute averages, except the Indiana site had hourly data.

[19] Feedback obtained from investigators at 12 of the 16 AmeriFlux sites indicated that most of the radiometers were calibrated annually, except the Arizona and British Columbia sites were calibrated approximately every two years. Topographic influence on incoming radiation was judged to be minimal or nonexistent based on investigator response and independent evaluation of the surrounding topography. Topography was most significant at the Washington site, with a large isolated hill located to the east extending approximately 13° above the horizon and a ridge to the south at approximately 9° above the horizon. The British Columbia site was located on a 6 to 9° east-facing slope. Niwot Ridge to the northwest of the Colorado site and the Santa Rita Mountains to the south of the Santa Rita, Arizona site extended approximately 8° above the horizon.

[20] For our initial analyses, a clearness index for each observation was computed based on a 24-hour window of observed incoming solar radiation centered on the observation. The influence of the length of the time over which solar observations were used to compute the clearness index was subsequently assessed. Clear-sky algorithms were initially evaluated without elevation correction (with the exception of interpolating for the Iziomon parameters) using observations when the clearness index was greater the 0.70 based on the range in clearness index suggested by *Campbell* [1985]. Although some cloud corrections were developed specifically for a certain clear-sky algorithm, all ten cloud corrections were paired with all 13 clear-sky algorithms to ascertain the best combination of algorithms for all-sky conditions. In some cases, this may have violated assumptions regarding maximum clear-sky emissivity and resulted in ε_a values greater than 1.0, suggesting that the coupling was incompatible. However, by matching all cloud corrections with all clear-sky algorithms, the best combinations could be identified, and any mismatching would presumably result in poorer model results.

[21] Model results were evaluated for mean bias difference (MBD), root mean square deviation (RMSD) and standard deviation (SD) of the 30-minute or hourly predictions, as well as RMSD of the predicted daily average fluxes ($RMSD_{daily}$). Ideally MBD and RMSD should approach zero and SD should mimic that of the observed values. RMSD can be separated into systematic ($RMSD_s$) and unsystematic ($RMSD_u$) errors. The systematic mean square deviation is evaluated as [*Willmott*, 1982]

$$MSE_s = N^{-1}\sum_{i=1}^{N}\left(\hat{P}_i - O_i\right)^2 \tag{7}$$

where $\hat{P}_i$ is obtained from the least squares linear regression between the predicted variable, P_i, and the observed variable, O_i, i.e., $\hat{P}_i = a + bO_i$. The unsystematic mean square deviation can be computed by difference: $MSE_u = MSE - MSE_s$. High $RMSD_s$ in relation to RMSD implies that the form of the model or algorithm could capture much of the observed variation after a simple linear correction to remove bias (perhaps by changing a coefficient). $RMSD_u$ is a measure of how accurate the model could be without a more complex nonlinear adjustment to the form of the model.

[22] The RMSD and SD of different algorithms were compared using an F test. Because the residuals for 30-minute and hourly estimates are strongly correlated, the number of independent samples is considerably less than the number of observations. Effective sample sizes were computed from the expression given by *Lee and Lund* [2004] adjusting for the lag-one autocorrelation of the residual time series.

$$n_e = n\left(\frac{1 - r(1) - 0.68n^{-1/2}}{1 + r(1) + 0.68n^{-1/2}}\right) \tag{8}$$

Here, n_e is the effective independent sample size for a given algorithm applied to a given site, n is the total number of observations for the site, and $r(1)$ is the lag-one autocorrelation of the times series of the residuals between measurements and the estimates. On the basis of this, each site typically had one to two independent samples for every 24 hours of observation.

4. Results

4.1. Clear-Sky Algorithms

[23] RMSD and MBD for each of the clear-sky algorithms without considering elevation corrections are given in Tables 5 and 6 for the initial 14 sites. The Ångström, Dilley and Prata algorithms stand out as being the best overall algorithms. The only site that the RMSD of the Prata algorithm was significantly higher ($p < 0.05$) than the best algorithm for that site was North Carolina; however, it was not significantly different at the $p < 0.01$ level. RMSD for the Ångström algorithm was significantly higher at $p < 0.05$ for the Arizona and North Carolina sites, but was not significant at $p < 0.01$. RMSD of the Dilley algorithm was significantly higher at $p < 0.01$ for the Arizona site. Except for the Yucheng, Mississippi and North Carolina sites, for which all algorithms overestimated L_{clr}, the Dilley algorithm tended to underestimate L_{clr} (Table 6), although its RMSD was among the best. Because of this bias, the systematic error ($RMSD_s$) of the Dilley algorithm was significantly higher than the Ångström and Prata algorithms. Conversely, its unsystematic error ($RMSD_u$) was the lowest, suggesting that it could perform best if the linear systematic error could be corrected. However, SD of the Dilley-predicted values is significantly different from the observed values, whereas the Ångström and Prata algorithms mimic the variability of the observed values quite well. Unsystematic error of the Garratt algorithm is similar to that of the Dilley algorithm, however its large negative MBD (Table 6) contributed to high RMSD and $RMSD_s$.

Table 5. Root Mean Square Deviations in Estimated Atmospheric Long-Wave Radiation (W m^{-2}) of Clear-Sky Algorithms for Each Site[a]

Site	Days	Ångström	Brunt	Brutsaert	Dilley	Garratt	Idso-1	Idso-2	Iziomon	Keding	Niemelä	Prata	Satterlund	Swinbank
Arizona	400	14.3	29.4	20.9	21.1	24.3	46.0	15.2	29.8	33.5	15.6	*12.6	22.3	43.9
BC	62	*16.2	23.8	*16.4	*15.3	22.3	*18.0	*20.8	*16.3	37.5	*17.3	*14.7	21.4	*18.0
Colorado	256	*22.8	34.8	32.6	*23.9	28.8	28.7	*24.7	59.3	54.3	30.7	*23.1	*23.9	28.9
Ganzi	118	*22.8	41.1	36.5	30.1	35.7	27.2	22.0	71.3	55.8	27.8	*24.3	*21.7	27.6
Idaho	283	*20.1	27.5	22.5	*18.9	22.8	30.3	22.7	39.9	36.2	22.9	*18.6	25.4	29.6
Indiana	129	*17.9	31.2	25.7	*20.6	28.4	*19.9	*20.4	*21.6	44.1	*19.3	*17.9	*20.1	22.7
Iowa	148	*22.3	34.5	29.0	*24.1	36.1	*25.9	*22.8	*26.1	43.0	*24.1	*21.8	*21.7	30.4
Mississippi	141	*36.7	*34.0	34.1	*29.8	*33.1	41.9	41.2	*33.2	51.9	39.7	*35.3	41.7	42.7
Nagqu	72	*28.7	39.1	*35.7	*31.5	*34.8	*34.8	*31.2	82.0	51.6	*36.7	*29.7	*29.6	*31.6
North Carolina	134	33.8	*24.6	*26.3	*24.5	*24.4	41.8	38.8	*27.0	47.2	37.9	31.3	40.1	39.2
South Dakota	174	*19.2	32.2	*27.7	*20.6	26.4	26.3	*20.5	39.1	43.4	*21.5	*18.9	*22.1	27.6
Washington	131	*19.2	28.9	20.9	*20.8	30.4	29.1	*21.8	*22.8	43.2	*21.2	*19.1	*22.7	29.8
Wisconsin	101	*23.7	35.4	*31.8	*23.7	31.7	*24.3	*25.9	*28.4	49.3	*25.1	*23.9	*24.7	*30.8
Yucheng	8	*31.7	*18.9	*20.1	*21.5	*20.2	*39.6	*37.0	*25.1	*42.5	*36.0	*28.7	*38.4	*35.2
All sites	2157													
RMSD		*23.5	31.1	27.2	*23.3	28.5	31.0	26.1	37.3	45.3	26.8	*22.9	26.8	31.3
$RMSD_s$		*10.9	22.9	15.2	15.0	21.4	17.7	16.5	29.7	29.9	15.4	*10.4	15.3	14.0
$RMSD_u$		20.9	21.0	22.5	*17.8	*18.8	25.5	20.2	22.5	33.9	22.0	20.3	22.0	28.0
SD		*54.8	*54.9	60.0	49.4	49.8	61.9	*54.1	59.5	85.1	*53.8	*53.6	57.3	68.4
$RMSD_{daily}$		*14.8	27.0	21.7	16.7	22.9	25.7	18.5	37.7	40.3	19.1	*13.9	19.5	24.7

[a]Asterisks indicate that the RMSD is not significantly different at the $p = 0.05$ level from the minimum RMSD for that site or that the standard deviation of predicted values is not significantly different from the observed standard deviation of 53.9 W m^{-2}.

[24] Clear-sky long-wave radiation was most accurately predicted for the Arizona site, which also had the most number of clear days. RMSD was not significantly higher for any of the algorithms for the Yucheng site, due in part to the small number of clear days. RMSD was highest for the North Carolina and Mississippi sites; with the exception of the Brunt and Garratt algorithms, which consistently underestimated L_{clr}, all algorithms overestimated L_{clr} for these sites. Algorithms tended to also overestimate L_{clr} for the Yucheng site.

[25] Idso-1 and Swinbank are the only algorithms that use only temperature to estimate L_{clr}. If humidity measurements are not available, there is no significant difference in RMSD between these two algorithms, however the systematic and bias errors of the Idso-1 algorithm are significantly higher than the Swinbank algorithm. An F test of the $RMSD_s$ and a paired t test of the MBD indicates that the Swinbank algorithm has a smaller MBD (5.3 W m^{-2}) and $RMSD_s$ (14.0 W m^{-2}) than the Idso-1 algorithm (MBD = +13.2 W m^{-2}; $RMSD_s$ = 17.7 W m^{-2}).

4.2. Elevation Corrections

[26] The data indicate little if any influence of elevation on predicted L_{clr}. In fact, correlations between MBD in Table 6 and elevation imply a negative slope, whereas without elevation correction, overprediction of L_{clr} is expected to increase with elevation. Ironically the highest elevation site, Ganzi, was among the sites that had the worst underprediction. The elevation correction developed by *Marks and Dozier* [1979] for the Brutsaert algorithm reduced estimated L_{clr} by an average of 1.1 W m^{-2} for the Washington site to 40.1 W m^{-2} for the Nagqu site. However, the Brutsaert algorithm already underpredicted L_{clr} for nearly all sites (Table 6), so the elevation correction only resulted in further underprediction. The *Deacon* [1970] elevation correction suggests a slope of 12 W m^{-2} per 1000 meters of elevation, depending on temperature. If the three sites that were consistently overpredicted (Yucheng, Mississippi and North Carolina) are ignored, the slopes of the MBD of Ångström, Dilley and Prata algorithms with

Table 6. Mean Bias Difference in Estimated Atmospheric Long-Wave Radiation (W m^{-2}) of Clear-Sky Algorithms for Each Site

Site	Days	Ångström	Brunt	Brutsaert	Dilley	Garratt	Idso-1	Idso-2	Iziomon	Keding	Niemelä	Prata	Satterlund	Swinbank
Arizona	400	6.0	−26.6	−15.5	−17.0	−20.8	34.2	8.7	−27.1	3.9	8.1	−0.1	17.3	31.4
BC	62	7.8	−18.6	−4.2	−5.9	−17.4	6.6	14.7	−7.7	27.5	8.6	2.5	15.7	3.5
Colorado	256	0.5	−27.1	−24.2	−11.0	−17.4	14.0	9.1	−55.2	−41.6	11.4	−0.8	7.2	1.0
Ganzi	118	−6.7	−34.8	−28.5	−20.6	−27.6	3.9	1.0	−67.5	−29.9	2.2	−9.6	0.4	−4.3
Idaho	283	8.2	−21.0	−12.2	−6.8	−14.0	20.5	13.9	−35.8	−5.7	11.6	4.0	16.9	12.9
Indiana	129	−0.3	−25.0	−13.8	−11.9	−23.0	4.3	8.7	−12.8	3.2	4.6	−3.3	7.8	−3.9
Iowa	148	−8.0	−26.6	−15.8	−15.6	−30.0	−2.1	7.2	−16.5	−0.7	4.1	−7.2	1.2	−12.3
Mississippi	141	15.2	−8.2	5.0	5.2	−8.4	15.1	25.6	5.6	30.2	19.3	12.1	23.5	8.8
Nagqu	72	2.0	−26.2	−21.8	−10.5	−17.3	12.5	10.1	−76.5	−31.2	11.9	−0.3	8.6	2.7
North Carolina	134	22.6	−4.3	5.2	9.4	0.4	28.8	30.5	11.5	14.8	27.4	19.2	30.6	22.4
South Dakota	174	1.4	−26.5	−19.5	−11.1	−19.0	12.6	8.6	−34.8	−21.2	6.8	−1.6	9.3	2.1
Washington	131	1.9	−21.5	−5.9	−12.2	−24.6	4.5	11.1	−13.2	32.3	6.0	−2.0	10.6	1.3
Wisconsin	101	−2.7	−25.8	−16.4	−8.8	−22.8	0.9	8.2	−16.4	−7.1	4.0	−4.7	4.0	−14.2
Yucheng	8	25.0	−2.8	7.4	11.7	2.5	29.5	31.8	15.1	20.7	28.5	20.7	32.6	23.1
All sites	2157	5.2	−21.1	−11.4	−7.5	−17.1	13.2	13.5	−23.7	−0.3	11.0	2.1	13.3	5.3

Table 7. Root Mean Square Deviations in Estimated Atmospheric Long-Wave Radiation (W m^{-2}) of All-Sky Conditions for All Sites Combined for Each Combination of Clear-Sky Algorithm and Cloud Correction[a]

	Cloud Corrections									
	Based on Cloud Cover								Based on Solar Index	
Clear-Sky Algorithm	Brutsaert	Iziomon	Jacobs	Kimball	Keding	Maykut	Sugita	Unsworth	Crawford	Lhomme
Ångström	*27.4	50.7	31.7	28.3	*26.9	*27.4	33.8	28.7	#25.3	28.9
Brunt	37.0	44.4	35.5	32.0	39.9	37.8	48.4	30.8	29.5	32.2
Brutsaert	33.5	49.6	35.6	29.3	33.9	33.8	40.4	30.0	26.6	31.4
Dilley	28.1	46.5	29.6	*26.2	29.2	28.7	37.4	*27.1	#24.9	*26.0
Garratt	34.0	39.9	29.9	32.7	38.8	35.3	49.1	29.6	29.7	28.5
Idso-1	32.5	52.5	36.3	33.8	32.9	32.4	39.5	32.6	30.4	34.5
Idso-2	35.8	65.1	44.2	32.8	30.8	34.9	30.8	31.7	27.5	40.2
Iziomon	42.8	46.3	42.4	37.3	44.8	43.4	52.6	35.1	33.7	39.0
Keding	50.1	74.2	57.7	45.6	45.2	49.2	43.5	39.9	36.1	53.3
Niemelä	35.5	61.1	42.4	32.4	32.4	34.8	34.6	31.9	28.4	38.6
Prata	29.1	51.3	33.3	*27.4	28.4	29.1	34.5	28.7	#25.1	29.7
Satterlund	30.9	58.1	38.0	31.1	27.8	30.3	31.4	30.9	26.8	34.8
Swinbank	34.3	49.7	36.3	34.3	35.9	34.5	43.3	32.4	30.6	34.5

[a]Clearness index was assumed to range from 0.4 to 0.7 for complete cloud cover to clear-sky conditions. (The pound signs indicate that the RMSD is not significantly different from the Dilley-Crawford combination; asterisks indicate that the RMSD is not significantly different from the RMSD of the Dilley-Kimball combination.)

elevation are essentially zero. Therefore an elevation correction was not considered further.

4.3. Estimates of Cloud Cover

[27] Algorithms presented by *Campbell* [1985] and *Kasten and Czeplak* [1980] for estimating cloud cover were compared. Each of the clear-sky algorithms in Table 1 was combined with each cloud-correction algorithm in Table 2 using both the cloud-estimation approaches of *Campbell* [1985] and *Kasten and Czeplak* [1980]. The RMSD for each combination is given in Table 7 using the approach of *Campbell* [1985]. The analyses in Table 7 assumed cloud cover ranged from 1.0 to 0.0 for a clearness index between $k_{cld} = 0.4$ and $k_{clr} = 0.7$ as suggested by *Campbell* [1985]. Of the algorithms that require an estimation of cloud cover, the lowest average RMSD over all sites was 26.2 W m^{-2} for the Kimball cloud correction combined with the Dilley clear-sky algorithm (Table 7). (The Crawford cloud correction stands out as being the best cloud correction when combined with the Ångström, Dilley or Prata clear-sky algorithms, but it does not require an estimate of cloud cover.) Using the cloud-estimation approach of *Kasten and Czeplak* [1980], the lowest average RMSD was 32.6 W m^{-2}, produced by a combination of the Dilley clear-sky algorithm and the Keding cloud correction. This is significantly larger than the RMSD produced using the approach of *Campbell* [1985]. The cloud-estimation approach of *Kasten and Czeplak* [1980] was therefore not considered further.

[28] Assumptions regarding cloud cover (c) and clearness index (k) were explored for the cloud-estimation approach of *Campbell* [1985] using the best clear-sky algorithms and cloud corrections from Table 7. Combinations not significantly different from the Dilley-Kimball combination were Ångström-Brutsaert, Ångström-Keding, Ångström-Maykut, and Dilley-Unsworth. Although the Prata algorithm was consistently one of the better clear-sky algorithms, these cloud corrections combined with the Prata clear-sky algorithm had significantly higher RMSD's than the Dilley-Kimball combination. Values of k_{cld} and k_{clr} in Campbell's cloud-estimation approach were evaluated for all combinations of these three clear-sky algorithms and five cloud corrections.

[29] Table 8 gives the RMSD of the Dilley-Kimball combined algorithm for all sites with various values of k_{cld} and k_{clr}. The best combination for clear skies and complete cloud cover was $k_{cld} = 0.25$ and $k_{clr} = 0.8$. This yielded a significantly lower RMSD than the original clearness indices of 0.4 and 0.7 in Table 7. Additionally, these optimum limits in clearness index (0.25, 0.8) did not have a significantly higher RMSD for any of the sites than the best combination for that site. The limits of 0.25 and 0.8 correspond closely with the limits in observed k for most sites. It is interesting to note that the cloud-estimation algorithm of *Kasten and Czeplak* [1980] yields similar limits in k for zero and complete cloud cover (0.2, 0.8) as the optimum limits (0.25, 0.8) found for the Dilley-Kimball combination in Table 8. However, the simple linear interpolation between k_{cld} and k_{clr} of the approach of *Campbell* [1985] yielded better results than the nonlinear approach of *Kasten and Czeplak* [1980].

Table 8. Influence of the Assumed Values of Clearness Index for Complete Cloud Cover (k_{cld}) and Clear Skies (k_{clr}) on RMSD of Estimated Atmospheric Long-Wave Radiation (W m^{-2}) of All-Sky Conditions for All Sites Combined[a]

	k_{cld}									
k_{clr}	0.00	0.05	0.10	0.15	0.20	0.25	0.30	0.35	0.40	0.45
0.55	33.1	32.3	31.5	30.6	29.9	29.2	28.7	28.3	28.1	28.2
0.60	31.8	31.1	30.2	29.4	28.7	28.1	27.6	27.3	27.2	27.4
0.65	30.7	29.9	29.1	28.3	27.6	27.0	26.6	26.4	26.5	26.9
0.70	29.5	28.8	28.0	27.3	26.6	26.2	25.9	***25.8**	26.2	26.6
0.75	28.5	27.8	27.1	26.4	25.8	***25.5**	***25.3**	***25.4**	***25.7**	26.5
0.80	27.7	27.0	26.3	***25.7**	***25.3**	***25.0**	***25.0**	***25.2**	***25.8**	26.8
0.85	27.1	26.5	25.9	***25.4**	***25.1**	***25.0**	***25.1**	***25.6**	26.4	27.6
0.90	26.7	26.2	***25.7**	***25.4**	***25.3**	***25.3**	***25.7**	26.3	27.3	28.7
0.95	26.6	26.2	25.8	***25.7**	***25.7**	25.9	26.4	27.2	28.3	29.8
1.00	26.7	26.3	26.1	26.1	26.2	26.6	27.2	28.1	29.3	30.9

[a]Values are for the Dilley clear-sky algorithm combined with the Kimball cloud correction. (Asterisks and bold face indicate that the RMSD is not significantly different at the $p = 0.05$ level from the minimum RMSD.)

Table 9. Optimum Values of k_{clr} and k_{cld} for Zero and Complete Cloud Cover to Minimize the RMSD of Various Combinations of the Best Clear-Sky Algorithms and Cloud Corrections

Clear-Sky Algorithm	Cloud Corrections				
	Brutsaert	Kimball	Keding	Maykut	Unsworth
		k_{cld}			
Ångström	0.25	0.25	0.40	0.25	0.15
Dilley	0.25	0.25	0.40	0.30	0.15
Prata	0.25	0.25	0.35	0.25	0.20
Suggested value for all clear-sky algorithms	0.25	0.25	0.35	0.25	0.20
		k_{clr}			
Ångström	0.80	0.70	0.80	0.95	0.70
Dilley	1.00	0.80	1.00	1.00	0.80
Prata	0.80	0.70	0.80	0.95	0.70

[30] The best combination of k_{cld} and k_{clr} for the three best clear-sky algorithms and the five best cloud corrections that use cloud cover c are presented in Table 9 based on an analysis similar to that in Table 8. Values for k_{cld} and k_{clr} selected in Table 9 for each combination of algorithms yielded an RMSD value for each site that was not significantly higher than for the optimum values of k_{clr} and k_{cld} for that site. The optimum limit for complete cloud cover, k_{cld}, was largely independent of the clear-sky algorithm used and a value was selected for each cloud cover correction (Table 9). The optimum value for k_{clr} varied with each combination of clear-sky algorithm and cloud cover correction.

4.4. Cloudy Sky Corrections

[31] The RMSD and MBD for combinations of the best clear-sky algorithms and cloud corrections using the values for k_{cld} and k_{clr} in Table 9 are given in Tables 10 and 11. (The RMSD's using the Keding and Maykut cloud corrections were significantly higher for nearly all sites and were therefore omitted from the tables for brevity. Although the Prata clear-sky algorithm was not significantly higher for many of the sites when combined with the Brutsaert, Kimball, or Unsworth cloud corrections, the averages for all sites were significantly higher, and it was therefore omitted for these three cloud corrections.) The Keding and Brutsaert cloud corrections occasionally yielded emissivities above 1.0; this occurred most often when combined with the Prata clear-sky algorithm, for which 1% and 3% of all emissivity estimates, respectively, were above 1.0. While summaries in Tables 10 and 11 include emissivities greater than 1.0 for these two cloud corrections, a separate analysis limiting predicted emissivities to 1.0 had little to no influence on the overall RMSD and MBD (maximum change of 0.2 W m^{-2} for the Dilley-Brutsaert combination).

[32] The algorithms that stand out as giving the best estimates for all sites are the Dilley clear-sky algorithm combined with the Kimball, Unsworth, or Crawford cloud correction and the Prata-Crawford combination. However, at the $p = 0.01$ level, the Unsworth and Crawford cloud corrections are not significantly higher when combined with any of the three best clear-sky algorithms. Of these combinations, the Ångström-Unsworth and Dilley-Unsworth yielded the lowest $RMSD_s$ (Table 10). Apparently optimizing the clearness indices in the Unsworth cloud correction compensated for the negative MBD and relatively high $RMSD_s$ of the Dilley clear-sky algorithm, giving this combination a relatively low $RMSD_s$. The lowest $RMSD_u$ was produced by the Dilley-Kimball algorithm.

[33] The four all-sky algorithms by Aubinet underestimated L_d for nearly all sites. MBD over all sites for the Aubinet algorithms was −4.3, −15.7, −21.4, and −10.7 W m^{-2}, respectively; RMSD was 29.5, 30.1, 36.0 and 27.8 W m^{-2}. The only sites that the RMSD of any of the Aubinet algorithms was not significantly higher than the best algorithm were Yucheng, Mississippi, and North Carolina,

Table 10. Root Mean Square Deviations in Estimated Atmospheric Long-Wave Radiation (W m^{-2}) of All-Sky Algorithms for Each Site Using the Optimum Values for k_{cld} and k_{clr} From Table 9[a]

Site	Days	Ångström-Brutsaert	Ångström-Kimball	Ångström-Unsworth	Ångström-Crawford	Dilley-Brutsaert	Dilley-Kimball	Dilley-Unsworth	Dilley-Crawford	Prata-Crawford
Arizona	721	17.7	18.5	17.8	17.7	19.2	*17.6	*17.4	21.2	*16.2
BC	713	*23.4	*23.3	*22.8	*22.9	*23.5	*23.5	*22.7	*23.1	*23.0
Colorado	714	*27.9	*28.0	*27.5	*27.3	*27.1	*26.0	*26.3	*26.1	*27.1
Ganzi	329	*26.6	*25.3	*25.3	*24.9	29.3	*27.2	*26.3	28.5	*26.0
Idaho	708	26.9	*26.2	*25.7	*25.8	*25.6	*24.1	*23.9	*24.6	*25.1
Indiana	708	24.0	25.1	*21.8	*22.2	24.9	*23.8	*21.2	*23.0	*21.7
Iowa	546	*23.8	*23.5	*22.3	*22.2	*23.4	*22.2	*21.2	*23.0	*21.7
Mississippi	669	30.5	31.1	29.5	29.3	30.0	27.5	28.4	*25.9	29.3
Nagqu	260	*28.9	*29.4	*30.3	*31.0	*30.1	*29.6	*31.0	*30.9	*31.4
North Carolina	688	29.7	32.0	29.5	30.0	*27.9	*28.5	*28.0	*25.9	28.9
South Dakota	611	*24.1	*24.4	*23.8	*23.7	*23.6	*22.6	*22.7	*22.6	*23.1
Washington	727	25.2	*23.8	*23.0	24.1	25.2	*24.0	*21.8	25.6	24.9
Wisconsin	607	26.8	*26.4	*24.4	*25.0	27.1	*25.6	*23.9	*25.1	*25.2
Yucheng	508	27.3	32.3	28.1	28.1	26.4	27.5	27.7	*23.4	27.1
All sites	7920									
RMSD		25.9	26.4	*25.1	25.3	26.0	*25.0	*24.5	*24.9	*25.1
$RMSD_s$		*10.5	12.5	*10.8	12.7	12.8	13.4	*10.7	14.0	11.7
$RMSD_u$		23.7	23.2	22.7	21.9	22.6	*21.1	22.0	*20.6	22.2
SD		*60.0	55.2	57.4	54.9	61.9	55.1	*58.1	55.6	57.4
$RMSD_{daily}$		16.8	17.0	*15.4	*15.6	17.4	*15.6	*14.9	*15.7	*15.1

[a]Asterisks indicate that the RMSD is not significantly different at the $p = 0.05$ level from the minimum RMSD for that site or that the SD of predicted values is not significantly different from the observed standard deviation of 59.0 W m^{-2}.

Table 11. Mean Bias Difference in Estimated Atmospheric Long-Wave Radiation (W m^{-2}) of All-Sky Algorithms for Each Site Using Optimum Values for k_{cld} and k_{clr} From Table 9

Site	Days	Ångström-Brutsaert	Ångström-Kimball	Ångström-Unsworth	Ångström-Crawford	Dilley-Brutsaert	Dilley-Kimball	Dilley-Unsworth	Dilley-Crawford	Prata-Crawford
Arizona	721	4.0	5.7	5.4	5.9	−9.7	−7.1	−4.1	−12.9	1.2
BC	713	−1.7	−0.4	1.4	−1.2	−6.0	−4.4	1.5	−6.4	−3.6
Colorado	714	−4.6	0.3	1.8	3.3	−10.8	−5.6	−0.4	−5.5	1.4
Ganzi	329	−11.2	−7.2	−6.7	−4	−17.9	−13.6	−9.5	−14.3	−6.5
Idaho	708	−2.0	2.1	2.8	3.4	−8.4	−3.9	−0.2	−6.7	−0.1
Indiana	708	−5.5	−8.4	−3.5	−5.7	−5.4	−9.8	−2.1	−10.4	−4.3
Iowa	546	−5.6	−6.3	−3.6	−5.3	−6.5	−8.6	−2.9	−10.7	−4.3
Mississippi	669	7.7	1.1	7.3	4.3	12.0	2.6	10.9	1.6	8.7
Nagqu	260	−2.4	3.0	4.7	7.1	−8.2	−2.3	3.6	−1.3	5.1
North Carolina	688	8.1	3.0	8.6	6.2	8.9	2.0	10.1	0.9	8.5
South Dakota	611	−2.5	2.0	2.8	4.1	−8.2	−3.0	1.6	−5.1	1.3
Washington	727	−9.3	−7.9	−6.7	−8.8	−12.9	−11.4	−6.8	−15.4	−11.2
Wisconsin	607	−7.9	−8.8	−4.6	−6.8	−5.6	−8.2	−1.6	−9.3	−6.2
Yucheng	508	13.0	5.4	13.6	10.8	14.2	4.5	15.7	6.7	13.3
All sites	7920	−1.4	−1.2	1.7	1.0	−4.6	−4.9	1.1	−6.3	0.2

which are the sites that the best algorithms tended to overestimate L_d. These are same three sites that the clear-sky algorithms overestimated L_{clr}.

4.5. Influence of Length of Solar Window for Estimating Clearness Index

[34] The previous analyses were based on clearness index being estimated using a 24-hour window of solar radiation centered on the 30-minute or hourly observation. More accurate estimates of L_d can likely be obtained, particularly for daytime values, by using a smaller window of observation. However, noontime values of L_d based on a single solar radiation value corresponding to the L_d observation yielded RMSD values higher than those using a 24-hour window of solar radiation. RMSD of noon values for L_d averaged over all sites for the five best algorithms in Table 10 using a single solar observation ranged from 20.4 to 22.3 W m^{-2} compared to 19.6 to 20.7 W m^{-2} using a 24-hour window. RMSD values using a single solar observation were significantly higher for all but the Prata-Crawford combination. The reason for significantly higher RMSD values is likely due to the fact that clouds covering the solar disk at the time of observation do not necessarily represent average conditions over the entire sky hemisphere. RMSD averaged over all sites reached a minimum when a 4-hour window for solar radiation around the L_d observation was used; RMSD values using the 4-hour window ranged from 19.3 to 20.6 W m^{-2}, which were not significantly lower than values using a 24-hour window of solar radiation. There was very little change in the RMSD for noon values when the solar radiation window was increased beyond eight hours. Clearly, stretching the solar observation window beyond sunrise and sunset would have no effect.

[35] The optimum window of solar radiation for estimating 06:00 and 18:00 L_d values was the first six to eight hours following sunrise and prior to sunset, respectively. However, this did not produce significantly lower RMSD's than the 24-hour window. Using a 24-hour window centered on the long-wave radiation observation worked best for the midnight observation.

[36] Significantly better estimates of L_d were obtained when the solar index was computed based on the average solar radiation over the period, rather than computing a clearness index for each solar observation, then computing an average clearness index over the solar observation window. This was likely due to the fact that small errors in observed solar radiation at low sun angles were weighted more heavily when averaging clearness index values than when averaging solar radiation values.

4.6. Diurnal Variation and Daily Average Estimates

[37] *Monteith* [1973] points out that many of the long-wave algorithms are based on average climatological conditions and may not be appropriate for diurnal variation. Indeed, the RMSD of predicted daily L_d ($RMSD_{daily}$ in Tables 5 and 10) computed from daily average observations is considerably lower than predictions for the 30-minute and hourly observations. $RMSD_{daily}$ values of 13.9 W m^{-2} for clear skies and 14.9 W m^{-2} for all-sky conditions are very near the instrument accuracy of 12 W m^{-2} reported by *Michel et al.* [2008]; thus, direct comparison between the very best algorithms is problematic for daily average fluxes.

[38] The algorithms were able to capture only a portion of the diurnal variation around the average L_d flux for a given day. The root mean square variation of observed L_d around the average flux for a day was 22.7 W m^{-2}. The fraction of the observed diurnal variation around the average daily flux explained by the algorithms was computed from

$$DE = 1 - \frac{\sum_{i=1}^{N}\sum_{j=1}^{M}\left[\left(P_{i,j} - \bar{P}_i\right) - \left(O_{i,j} - \bar{O}_i\right)\right]^2}{\sum_{i=1}^{N}\sum_{j=1}^{M}\left[O_{i,j} - \bar{O}_i\right]^2} \tag{9}$$

where DE is defined here as the diurnal efficiency and can range from negative infinity to 1.0, $\bar{P}_i$ and $\bar{O}_i$ are the average predicted and observed fluxes for day i, and subscript j refers to each 30-minute or hourly observation. DE ranged from 0.21 to 0.28 for the best algorithms, indicating that the 30-minute or hourly estimates capture the diurnal variation slightly better than the average estimate for the day. Thus the algorithms have some capability for predicting diurnal variation, but it is marginal.

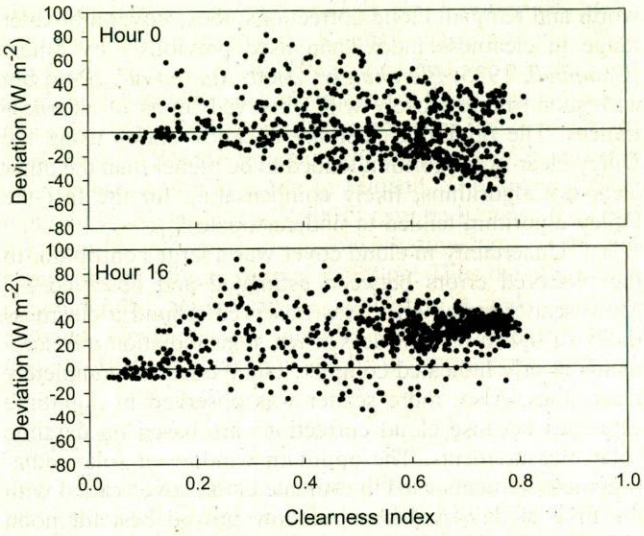

Figure 1. Deviation between estimated and measured incoming long-wave radiation (L_d) versus clearness index at hours 0:00 and 16:00 for the Mississippi site.

4.7. Daytime Versus Nighttime Estimates

[39] For nearly all sites, daytime estimates of L_d were better than nighttime estimates. As indicated earlier, the RMSD of noon estimates ranged from 19.3 to 20.6 W m^{-2} for the five best algorithms in Table 10 using a 4-hour solar window; midnight estimates of L_d ranged from 25.0 to 25.6 W m^{-2}. Greater daytime accuracy can be attributed to more uncertainty in cloud cover during nighttime compared to daytime and fewer surface inversions during daytime.

[40] Notable exceptions to more accurate daytime estimates were observed around hour 16:00 at the Yucheng, North Carolina and Mississippi sites. Typical RMSD's for 16:00 at these sites for the five best algorithms were 29 to 33 W m^{-2} compared to 24 to 28 W m^{-2} for the midnight values. Also, while MBD of midnight estimates were within 5 W m^{-2} of that for hour 16:00 for most sites, the MBD increased by around 12 W m^{-2} for the Yucheng and North Carolina sites and 24 W m^{-2} for the Mississippi site. Interestingly, these are the same sites that were consistently overpredicted by the clear-sky algorithms (Table 6). MBD of all nighttime estimates for these sites using the five best algorithms are similar to the midnight hour, while the MBD for daytime estimates gradually increase from nearly no bias at around 6:00 to a maximum bias at around 15:00 to 16:00, then back to nearly no bias at around 20:00 to 21:00. Figure 1 displays the error of the Dilley-Unsworth algorithm, which is typical of the five best algorithms, with varying clearness index at hours 0:00 and 16:00. Inspection of this plot indicates that the daytime bias is more severe on relatively clear days (clearness index greater than 0.6) than on cloudy days. At full cloud cover (clearness index less than 0.2), estimates show very little error compared to measured values. However, the error is clustered around +40 W m^{-2} when the clearness index exceeds 0.6. As is typical of all sites, there is more scatter in the error around a clearness index of 0.4; this is likely due to the fact that there is more uncertainty in cloud conditions around 50% cover than when solar radiation measurements indicate either obviously clear or cloudy skies. The bias in measured L_d at the Mississippi, North Carolina and Yucheng sites above a clearness index of 0.6 may suggest a bias in either long-wave radiation measurements or temperature measurements when there is strong solar radiation loading. Therefore the apparent bias in the long-wave radiation estimates for these three sites may be a problem with the instruments rather than a problem with the algorithms.

4.8. Test of Algorithms on Independent Sites

[41] Table 12 summarizes the results for best algorithms tested on a set of sites independent of the optimized clearness indices. The Dilley clear-sky algorithm combined with either the Kimball, Unsworth, or Crawford cloud correction again yielded significantly lower RMSD than other algorithms for both half-hourly and daily observations. Interestingly, the Dilley-Crawford algorithm, which required no prior optimization of the clearness indices, had the lowest RMSD for nearly every site and one of the best MBD's. This algorithm along with the Dilley-Kimball

Table 12. Root Mean Square Deviations in Estimated Atmospheric Long-Wave Radiation (W m^{-2}) of the Best All-sky Algorithms Applied to a Set of Independent Sites[a]

Site	Days	Ångström-Brutsaert	Ångström-Kimball	Ångström-Unsworth	Ångström-Crawford	Dilley-Brutsaert	Dilley-Kimball	Dilley-Unsworth	Dilley-Crawford	Prata-Crawford
Alaska[b]	348	*38.9	*38.2	*37.1	*36.4	*36.4	*35.7	*34.5	*34.7	*35.8
Arizona	685	28.6	29.6	29.3	29.7	*23.4	*23.5	*24.5	*23.4	28.1
Illinois	333	27.9	27.4	*27.0	*26.6	*27.1	*25.1	*26.1	*23.7	*26.0
Missouri	727	24.7	24.9	24.1	*23.5	*23.1	*22.1	*22.7	*21.5	*22.7
Montana	670	36.2	37.1	36.6	36.4	*31.8	*32.9	34.4	*30.3	34.4
South Dakota	689	28.2	*27.0	*26.6	*26.2	*26.9	*25.1	*25.3	*24.8	*26.4
Tennessee	414	*22.7	24.2	*21.6	*22.0	*22.5	*22.6	*20.5	*22.2	*20.8
All sites	7732									
RMSD		29.6	29.8	28.9	28.7	27.3	*26.7	*26.9	*25.8	27.7
$RMSD_s$		9.2	11.7	11	12.2	*7.6	10.3	9.6	10.4	10.5
$RMSD_u$		27.7	26.9	26.2	25.4	25.9	*24.4	24.7	*23.5	25.2
SD		*64.9	*61.7	*62.9	60.7	*65.1	60.7	*63.1	60.1	*62.4
$RMSD_{daily}$		20.6	20.3	19.4	18.9	17.9	*16.6	*17.0	*15.7	17.6
MBD		4.0	4.5	6.6	5.6	1.2	1.0	6.1	−1.3	4.6

[a]Asterisks indicate that the RMSD is not significantly different at the $p = 0.05$ level from the minimum RMSD for that site or that the SD of predicted values is not significantly different from the observed standard deviation of 63.4 W m^{-2}.
[b]Values for Alaska site include spring and summer data only.

algorithm also had significantly lower unsystematic errors. However, the Dilley-Crawford algorithm yielded estimates with significantly lower SD than the observed values.

[42] RMSD tended to be highest for the Alaska site and MBD was typically around -10 W m^{-2}. Estimates for the Alaska site were limited to spring and summer observations because the clearness index becomes undefined for a portion of the fall and winter months. Using a clearness index of 0.5 for the fall-winter months yielded an RMSD of 36.5 W m^{-2} for the Dilley-Unsworth algorithm compared to 34.5 W m^{-2} for the spring-summer months using the computed clearness index (Table 12) and 40.5 W m^{-2} for the spring-summer months using a clearness index of 0.5.

[43] Estimates for the Montana site had somewhat higher RMSD compared to most other sites (Table 12) and tended to overpredict L_d. MBD of the best algorithms ranged from +8 to +16 W m^{-2} for the Montana site and the diurnal shift in bias exhibited the same trend as the Mississippi, North Carolina and Yucheng sites.

5. Discussion and Conclusions

[44] The Dilley, Prata and Ångström algorithms were the best clear-sky algorithms. The Dilley and Prata algorithms were the only ones based on precipitable water as a predictive factor, though the estimate of precipitable water is here based on a ratio of e_0 and T_0 [*Prata*, 1996], while the Ångström algorithm for clear-sky emissivity was based solely on vapor pressure. The Idso-1 and Swinbank models, which are the only two models based solely on temperature, did the poorest. The study performed by *Hatfield et al.* [1983] also found that the temperature-based algorithms compared poorly to other algorithms. *Hatfield et al.* [1983], who did not evaluate the Dilley, Prata or Ångström algorithms, found a form of the Brutsaert equation performed best in their analysis of 15 locations; the Brutsaert algorithm ranked fourth in the present analysis based on RMSD.

[45] Efforts to include an elevation correction in the clear-sky algorithms proved fruitless. Extrapolating coefficients from two elevations provided by *Iziomon et al.* [2003] did not work outside the range observed in their study. The Iziomon algorithm performed reasonably at lower elevations, but was one of the worst algorithms for elevations above 1489 m, the elevation of their highest site. The elevation correction developed by *Marks and Dozier* [1979] for the Brutsaert algorithm reduced estimated L_{clr} by an average of 40.7 W m^{-2} for the highest elevation, however the Brutsaert algorithm already underpredicted L_{clr} for nearly all sites. *Marks and Dozier* [1979] also noted a systematic underprediction of L_{clr} using the elevation-corrected Brutsaert algorithm. The elevation correction suggested by *Deacon* [1970] appeared to overemphasize the effect of elevation. Correlations between MBD and elevation provided no evidence of an elevation effect. One might conclude that the error in the algorithms and uncertainty in the measurements may overshadow the influence of elevation on L_d.

[46] The cloud-correction algorithms of Kimball, Unsworth and Crawford described the data best and are recommended for most sites. These performed best when combined with the Dilley clear-sky algorithm. Limits in the clearness index of 0.20 to 0.25 for complete cloud cover and 0.8 for clear skies are suggested herein for the Unsworth and Kimball cloud corrections; these cover a broader range in clearness index than used previously by others [*Campbell*, 1985; *Flerchinger*, 2000; *Xiao et al.*, 2006] but correspond more closely with observed limits in clearness indices. The optimum clear-sky clearness index using the Dilley clear-sky algorithm tended to be higher than the other clear-sky algorithms, likely compensating for the fact the Dilley algorithm tended to underestimate L_{clr}.

[47] Uncertainty in cloud cover was a large contributor to the observed errors between estimated and observed L_d. More scatter in the error was observed around a clearness index of 0.4 to 0.5 and less when solar radiation measurements clearly indicated complete cloud cover or completely clear skies. Also, more scatter was observed in nighttime estimates because cloud corrections are based on daytime solar measurements. The optimum window of solar radiation measurements used to estimate cloud cover varied with the time of day. A 4-hour window proved best for noon estimates; the first six to eight after sunrise or before sunset gave the lowest RMSD for estimates around dawn and dusk; and a 24-hour window centered around the observed L_d gave the best result for midnight observations. However, the optimum window for the noon estimates and estimates near dawn and dusk were not significantly better than using a 24-hour window.

[48] Although the algorithms do not specifically address cloud type, haze and turbidity of the atmosphere, these contributions to incident long-wave radiation are indirectly compensated for because the more they influence measured solar radiation, the more they will contribute to incident long-wave radiation. One might conjecture whether changes in atmospheric CO_2 have influenced atmospheric long-wave radiation, however *Kessler and Jaeger* [2003] found no marked change in a 27-year record in Germany. One clear limitation with the presented approaches is application during winter at extreme latitudes where cloud conditions must be based on very short or nonexistent daylight, as with the Alaska site.

[49] RMSD of daily estimates were as low as 14.9 W m^{-2} compared to 24.5 W m^{-2} for 30-minute and hourly estimates of L_d. Clearly the algorithms had difficulty capturing the diurnal variation (typically 22.7 W m^{-2}) around the daily average flux. A portion of the higher RMSD for 30-minute estimates can be attributed to more uncertainty in cloud conditions for 30-minute predictions, but the RMSD of 19.3 W m^{-2} for noontime predictions using a 4-hour solar window, when estimated cloud conditions would presumably have more certainty, is still appreciably higher than $\text{RMSD}_{\text{daily}}$ values in Table 10. Another likely cause for difficulty in predicting diurnal variation in L_d is rapid air temperature changes with height near the surface due to diurnal heating and cooling.

[50] Observed RMSD for half-hourly or hourly estimates from the best algorithms over all sites (22.9 W m^{-2} for clear-sky conditions and 24.5 W m^{-2} for all-sky conditions, or about 8% of observed L_d) are comparable to other studies where algorithms were calibrated for specific sites. *Lhomme et al.* [2007] developed a relation for two sites in Bolivia that yielded an RMSD of 27 to 28 W m^{-2}; *Marks and Dozier* [1979] presented a relationship for clear-sky conditions in the southern Sierra Nevada Mountains with an RMSD of 26 to 31 W m^{-2} over the two years of that

analysis. *Alados-Alboledas et al.* [1995] reported 6% accuracy for a modification of the Kimball algorithm for a site in Spain. *Iziomon et al.* [2003] also reported 6% accuracy for an algorithm calibrated for two sites in Germany. However, *Niemelä et al.* [2001] reported somewhat better results of 11.8 W m^{-2} RMSD for midnight estimates of L_d using a derived expression at a site in Finland. The lower RMSD reported by *Niemelä et al.* [2001] may be because they had the benefit of visual cloud observations and were not attempting to capture diurnal variation. Thus the algorithms recommended herein can be applied to a wide range of climates, elevations and latitudes with accuracy similar to that reported for algorithms calibrated for specific sites.

Appendix A

[51] Clear-sky solar radiation at the earth's surface (S_{clr}) was calculated using a model presented by *Crawford and Duchon* [1999] based on the results of *Paltridge and Platt* [1976] and *Meyers and Dale* [1983] where instantaneous S_{clr} is approximated by

$$S_{clr} = S_0(\sin\alpha)\tau_R\tau_{pg}\tau_w\tau_a \tag{A1}$$

for positive solar altitude angles, α, which is the angle of the sun above the horizon. Here, S_o is the solar constant (taken as 1360 W m^{-2}) and τ_R, τ_{pg}, τ_w, and τ_a are transmission coefficients for Rayleigh scattering, absorption by permanent gases, absorption by water vapor, and absorption and scattering by aerosols. The empirical expression for the product of the first two transmission coefficients is

$$\tau_R\tau_{pg} = 1.021 - 0.084[m(0.00949P + 0.051)]^{0.5} \tag{A2}$$

where P is the pressure (kPa) and m is the optical air mass at 101.3 kPa given by $m = 35\sin\alpha(1224\sin^2\alpha + 1)^{-0.5}$. The transmission coefficient for absorption by water vapor is

$$\tau_w = 1 - 0.077(wm)^{0.3} \tag{A3}$$

where w is precipitable water defined in Table 1. The transmission coefficient for aerosols is

$$\tau_a = 0.935^m. \tag{A4}$$

The solar altitude angle is computed from

$$\sin\alpha = \sin\lambda\sin\delta + \cos\lambda\cos\delta\cos(\pi(t - t_{noon})/12) \tag{A5}$$

where λ is the latitude of the site, δ the solar declination, and t_{noon} is the time of solar noon. Solar declination is computed from

$$\delta = 0.4102\sin\left(\frac{2\pi}{365}(J - 80)\right). \tag{A6}$$

where J is the day of the year. Values for S_{clr} for each 30-minute or hourly observation of L_d were obtained from averaging equation (A1) over a 24-hour period surrounding the observation.

[52] **Acknowledgments.** The authors express gratitude to the AmeriFlux research community for making the data used herein publicly available. In particular, we would like to thank Russell Scott (AZ), Tom Kolb (AZ), Sabina Dore (AZ), Walter Oechel (AK), T. Andy Black (BC), Michael Novak (BC), Russell Monson (CO), Sean Burns (CO), Tilden Meyers (IL, MO, MT, MS, SD and TN), Danilo Dragoni (IN), Hans Peter Schmid (IN), Lianhong Gu (MO), Stephen Pallardy (MO), Paul Hanson (MO), Gabriel Katul (NC), Ram Oren (NC), Kyaw Tha Paw U (WA), Ken Davis (WI), and Paul Bolstad (WI) for providing the relatively complete, high-quality data sets to the AmeriFlux Web site. Measurements at Willow Creek, Wisconsin, were supported by the U.S. Department of Energy's Office of Science (BER) through the Midwestern Regional Center of the National Institute for Global Environmental Change. The Office of Science (BER), U.S. Department of Energy also supported research at the Morgan Monroe State Forest (Grant DE-FG02-95ER62083) and Duke Forest (Grant DE-FG02-07ER64371).

References

Alados-Alboledas, L., J. Vida, and F. J. Olmo (1995), The estimation of thermal atmospheric radiation under cloudy skies, *Int. J. Clim.*, *15*, 107–116.

Ångström, A. (1918), A study of the radiation of the atmosphere, *Smithson. Misc. Collect.*, *65*, 1–159.

Aubinet, M. (1994), Longwave sky radiation parameterizations, *Sol. Energy*, *53*, 147–154.

Brunt, D. (1932), Notes on radiation in the atmosphere, *Q. J. R. Meteorol. Soc.*, *58*, 389–420.

Brutsaert, W. (1975), On a derivable formula for long-wave radiation from clear skies, *Water Resour. Res.*, *11*, 742–744.

Brutsaert, W. (1982), *Evaporation into the Atmosphere*, 299 pp., Springer, New York.

Campbell, G. S. (1985), *Soil Physics with Basic: Transport Models for Soil-Plant Systems*, Elsevier, New York.

Crawford, T. M., and C. E. Duchon (1999), An improved parameterization for estimating effective atmospheric emissivity for use in calculating daytime downwelling longwave radiation, *J. Appl. Meteorol.*, *48*, 474–480.

Deacon, E. L. (1970), The derivation of Swinbank's long-wave radiation formula, *Q. J. R. Meteorol. Soc.*, *96*, 313–319.

Dilley, A. C., and D. M. O'Brien (1998), Estimating downward clear sky long-wave irradiance at the surface from screen temperature and precipitable water, *Q. J. R. Meteorol. Soc.*, *124*, 1391–1401.

Duarte, H. F., N. L. Dias, and S. R. Maggiotto (2006), Assessing daytime downward long-wave radiation estimates for clear and cloudy skies in Southern Brazil, *Agric. Forest Meteorol.*, *139*, 171–181.

Edwards, J. M., and A. Slingo (1996), Studies with a flexible new radiation code. I: Choosing a configuration for a large-scale model, *Q. J. R. Meteorol. Soc.*, *122*, 689–719.

Finch, J. W., and M. J. Best (2004), The accuracy of downward short- and long-wave radiation at the earth's surface calculated using simple models, *Meteorol. Appl.*, *11*, 33–39.

Flerchinger, G. N. (2000), *The Simultaneous Heat and Water (SHAW) Model: Technical Documentation*, *Tech. Rep. NWRC-2000-09*, USDA-ARS, Northwest Watershed Research Center, Boise, Idaho. (Available at: http://www.ars.usda.gov/Services/docs.htm?docid=16931)

Garratt, J. A. (1992), Extreme maximum land surface temperatures, *J. Appl. Meteorol.*, *31*, 1096–1105.

Hatfield, J. L., R. J. Reginato, and S. B. Idso (1983), Comparison of long-wave radiation calculation methods over the United States, *Water Resour. Res.*, *19*, 285–288.

Idso, S. B. (1981), A set of equations for full spectrum and 8 to 14 μm and 10.5 to 12.5 μm thermal radiation from cloudless skies, *Water Resour. Res.*, *17*, 295–304.

Idso, S. B., and R. D. Jackson (1969), Thermal radiation from the atmosphere, *J. Geophys. Res.*, *74*, 5397–5403.

Iziomon, M. G., H. Mayer, and A. Matzarakis (2003), Downward atmospheric longwave irradiance under clear and cloudy skies: Measurement and parameterization, *J. Atmos. Sol. Terr. Phys.*, *65*, 1107–1116.

Jacobs, J. D. (1978), Radiation climate of Broughton Island, in *Energy Budget Studies in Relation to Fast-Ice Breakup Processes in Davis Strait* (*Occas. Pap. 26*), pp. 105–120, Univ. of Colorado, Inst. of Arctic and Alp. Res., Boulder, Colo.

Kasten, F., and G. Czeplak (1980), Solar and terrestrial radiation dependent on the amount and type of cloud, *Sol. Energy*, *24*, 177–189.

Keding, I. (1989), Klimatologische Untersuchung über die atmosphärische Gegenstrahlung und Vergleich von Berechnungsverfahren anhand langjähriger Messungen im Oberrheintal, *Ber Dtsch. Wetterd*, *178*, 72 pp.

Kessler, A., and L. Jaeger (2003), Analysis of long time series of long-wave radiation fluxes above a pine forest, *Theor. Appl. Climatol.*, *74*, 179–189.

Kimball, B. A., S. B. Idso, and J. K. Aase (1982), A model of thermal radiation from partly cloudy and overcast skies, *Water Resour. Res.*, *18*, 931–936.

Lee, J., and R. Lund (2004), Revisiting simple linear regression with autocorrelation errors, *Biometrika*, *91*, 240–245.

Lhomme, J. P., J. J. Vacher, and A. Rocheteau (2007), Estimating downward long-wave radiation on the Andean Altiplano, *Agric. Forest Meteorol.*, *145*, 139–148.

Marks, D., and J. Dozier (1979), A clear-sky longwave radiation model for remote alpine areas, *Arch. Meteorol. Geophys. Bioklimatol. Ser. B*, *27*, 159–187.

Maykut, G. A., and P. F. Church (1973), Radiation climate of Barrow, Alaska, 1962–66, *J. Appl. Meteorol.*, *12*, 620–628.

Meyers, T. P., and R. F. Dale (1983), Predicting daily insolation with hourly cloud height and coverage, *J. Clim. Appl. Meteorol.*, *22*, 537–545.

Michel, D., R. Philipona, C. Ruckstuhl, R. Vogt, and L. Vuilleumier (2008), Performance and uncertainty of CNR1 net radiometers during a one-year field comparison, *J. Atmos. Ocean Technol.*, *25*, 442–451.

Monteith, J. L. (1973), The radiation environment, chap. 3, in *Principles of Environmental Physics*, Elsevier, New York.

Niemelä, S., P. Räisänen, and H. Savijärvi (2001), Comparison of surface radiative flux parameterizations. part I: Longwave radiation, *Atmos. Res.*, *58*, 1–18.

Orsini, A., F. Calzolari, T. Georgiadis, V. Levizzani, M. Nardino, R. Pirazzini, R. Rizzi, R. Sozzi, and C. Tomasi (2000), Parameterisation of surface radiation flux at an Antarctic site, *Atmos. Res.*, *54*, 245–261.

Paltridge, G. W., and C. M. R. Platt (1976), *Radiative Processes in Meteorology and Climatology*, 318 pp., Elsevier, New York.

Pérez-García, M. (2004), Simplified modelling of the nocturnal clear sky atmospheric radiation for environmental applications, *Ecol. Modell.*, *180*, 395–406.

Pope, V. D., M. L. Gallani, P. R. Rowntree, and R. A. Stratton (2000), The impact of new physical parameterizations in the Hadley Centre climate model: HadAM3, *Clim. Dyn.*, *16*, 123–146.

Prata, A. J. (1996), A new long-wave formula for estimating downward clear-sky radiation at the surface, *Q. J. R. Meteorol. Soc.*, *122*, 1127–1151.

Satterlund, D. R. (1979), An improved equation for estimating longwave radiation from the atmosphere, *Water Resour. Res.*, *15*, 1649–1650.

Sugita, M., and W. Brutsaert (1993), Cloud effect in the estimation of instantaneous downward longwave radiation, *Water Resour. Res.*, *29*, 599–605.

Swinbank, W. C. (1963), Long-wave radiation from clear skies, *Q. J. R. Meteorol. Soc.*, *89*, 339–348.

Unsworth, M. H., and J. L. Monteith (1975), Long-wave radiation at the ground, *Q. J. R. Meteorol. Soc.*, *101*, 13–24.

Willmott, C. J. (1982), Some comments on evaluation of model performance, *Bull. Am. Meteorol. Soc.*, *63*, 1309–1313.

Xiao, W., G. N. Flerchinger, Q. Yu, and Y. Zheng (2006), Evaluation of SHAW model in simulating the components of net all-wave radiation, *Trans. ASABE*, *49*, 1351–1360.

G. N. Flerchinger and D. Marks, USDA Agricultural Research Service, Northwest Watershed Research Center, 800 Park Boulevard, Suite 105, Boise, ID 83712, USA. (gerald.flerchinger@ars.usda.gov)

T. J. Sauer, National Soil Tilth Laboratory, USDA Agricultural Research Service, 2110 University Boulevard, Ames, IA 50011-3120, USA.

W. Xaio and Q. Yu, Institute of Geographical Sciences and Natural Resources Research, Chinese Academy of Sciences, No. 11A Datun Road, Beijing 100101, China.